The International Journal of Advanced Manufacturing Technology (2019) 102:3065–3076
https://doi.org/10.1007/s00170-019-03388-9

ORIGINAL ARTICLE

Study of friction stir butt welding between thin plates of AA5754 and mild steel for automotive applications

P. N. Karakizis[1] · D. I. Pantelis[1] · D. A. Dragatogiannis[2] · V. D. Bougiouri[1] · C. A. Charitidis[2]

Received: 16 April 2018 / Accepted: 21 January 2019 / Published online: 11 February 2019

Abstract
In the present study, the feasibility of joining 2 mm thick plates of AA5754-H114 to mild steel was examined. Sound friction stir dissimilar butt welding was achieved between thin plates of the automotive grade 5754 aluminum alloy and mild steel for the first time. Moderate rotational speed and a rather slow traverse speed were used. The mechanical properties of the weld were close to the equivalent of the aluminum base metal and a rise in the microhardness of the weld nugget of around 40% compared to the equivalent of the mild steel base metal was presented. An interdiffusion layer with a width of around 5 μm was created at the interface of the two alloys, the extended width of which probably affects positively the mechanical properties of the welds.

Keywords Friction stir welding · Dissimilar welding · Mild steel · AA5754 · Microstructure · Mechanical behavior

1 Introduction

During the last decades, the industrial demand to reduce the weight of structures, machines, and mechanical components has increased exponentially. As a result, a lot of steel components have been substituted with equivalent ones made from lighter metals such as aluminum alloys. Nevertheless, there are cases, especially in structural parts of machinery and constructions, where the extremely high strength of steel is irreplaceable. As a result, the need to weld steel to aluminum has arisen. For example, in the shipbuilding industry, the hull of most ships is made of steel, while the superstructure is made of aluminum, in order to keep the center of mass low for better stability and buoyancy. In the automotive industry, most manufacturers are also starting to consider substituting the steel car shell (or some parts of it) with a lighter aluminum alloy one. More specifically, General Motors™ is planning to eliminate rivets that join an aluminum bracket to the steel framework to form part of the seatback for the new Cadillac CT6™. However, most fusion welding methods fail to achieve good bonding between the two aforementioned materials, especially due to their different melting point, at least without the use of very expensive noble metal inserts. On the other hand, friction stir welding (FSW), a solid-state welding method that was invented by the welding institute (TWI) of the UK in 1991 [1], is very promising for successfully joining materials that are difficult to weld by the conventional fusion methods such as the AA7020-T6 [2] and the AA6082-T6 [3, 4] including dissimilar material combinations such as the FSW of AA6082-T6 to AA7075-T651 [5] and the FSW of AA5083-H111 to AA6082-T6 [6]. In the recent years, a lot of research has been conducted regarding the incorporation of ceramic particles in the weld seam of similar [7] as well as dissimilar materials [7–10] via friction stir processing (FSP) [11], a derivative of FSW.

Nevertheless, in the last 10 years, the feasibility of the dissimilar FSW between aluminum and steel has been moderately studied. The first published study was from Uzun et al. [12] and it concerned the FSW of AA6013-T4 to X5CrNi18-10 stainless steel. Although the fatigue testing showed a 30% reduction in results compared to the ones with AA6013-T6 as base metal, no tensile testing results were provided. The first study regarding the FSW of aluminum to structural steel was conducted by Jiang et al. [13]. The authors managed to achieve sound welding between 6061 Al alloy and AISI 1018 steel. During the

✉ P. N. Karakizis
karakizisp@gmail.com

[1] Shipbuilding Technology Laboratory, School of Naval Architecture and Marine Engineering, National Technical University of Athens, 9 Heroon Polytechniou st., Zografos, GR-157 80 Athens, Greece

[2] Laboratory Unit of Nanomechanics and Nanoengineering, School of Chemical Engineering, National Technical University of Athens, 9 Heroon Polytechniou st., Zografos, GR-157 80 Athens, Greece

Table 1 Chemical composition of the 5754 aluminum alloy and the mild steel (wt%)

	Al	Fe	Mn	Mg	P	S	Si	C
AA5754	Bal.	0.4	0.5	2.6–3.2	–	–	0.4	–
Mild steel	–	Bal.	0.6–0.9	–	≤0.04	≤0.05	–	0.14–0.20

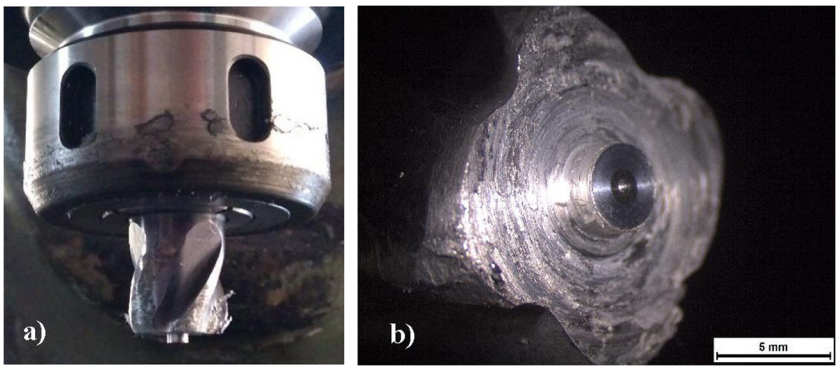

Fig. 1 Macrographs of the cemented carbide tool. **a** On the tool holder. **b** Tool pin close-up

tensile testing, the specimens did not fracture at the weld nugget (WN), something that also indicates that the weld was sound. Watanabe et al. [14] welded 2-mm-thick AA5083 plates to SS400 mild steel. The maximum tensile strength achieved was around 14% lower than the equivalent of the AA5083 base metal. Unfortunately, the stress-strain diagrams were not provided, and as a result, no robust conclusions on the elongations of the specimens can be drawn. Tanaka et al. [15] studied the intermetallic layer that is formed at the Al-steel interface during FSW and concluded that its thickness is inversely proportional to the joint strength. Nevertheless, the aforementioned joint strength was lower than the equivalent of the FSWed AA7075-T6.

Table 2 FSW experiments' parameters

Set	Experiment	Traverse speed (mm/min)	Rotational speed (RPM)
1	1	30	475
	2	30	600
	3	30	750
	4	30	950
2	1	47.5	600
	2	47.5	750
	3	47.5	950
3	1	60	750
	2	60	950
4	1	75	750
	2	75	950

More recently, Sajan et al. [16] tried the FSW of thicker (6 mm) AA6082 plates to mild steel but the presence of voids and pores on the aluminum side could not be eliminated resulting in bad tensile performance. Also, Thomä et al. [17] and Tang et al. [18] have successfully used ultrasound and preheating, respectively, in order to achieve better weldability between the two materials.

In the present study, the feasibility of joining 2-mm-thick plates of AA5754-H114 to mild steel is going to be examined. The study is focused on the welds' microstructure, microhardness, and mechanical properties (e.g., tensile testing). The two aforementioned materials are widely used in the automotive industry. Achieving a sound welding between them can lead to the reduction of the overall weight of cars, of their fuel consumption, and consequently of their CO_2 emissions. Additionally, the range of electric cars can be extended. To the best of the author's knowledge, no such study has ever been published internationally.

2 Experimental procedure

2.1 Materials used

The automotive grade 5754 aluminum alloy in the H114 strain hardened condition was welded with mild steel. The nominal chemical compositions of the two materials are presented in Table 1. The original dimensions of the plates to be welded were 200 × 100 × 2 mm^3.

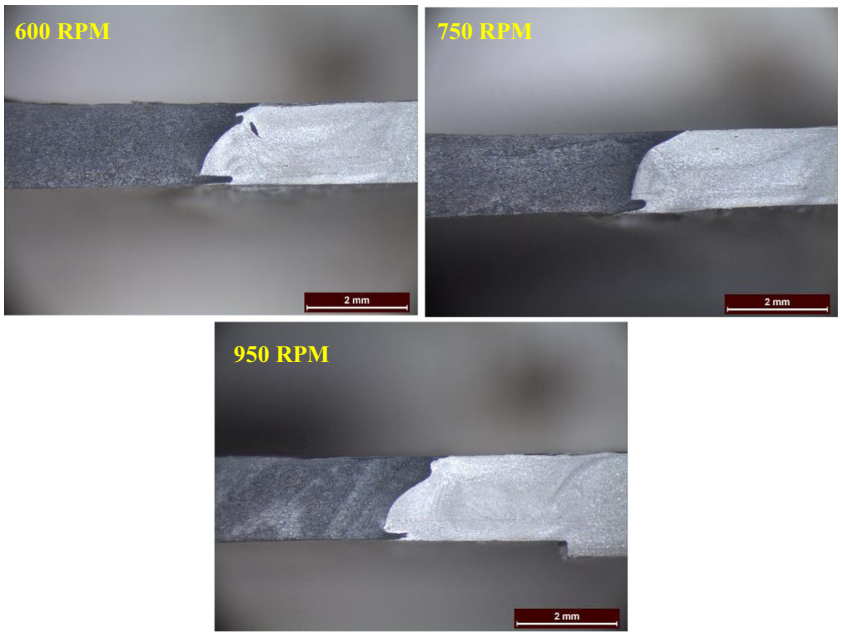

Fig. 2 Optical macrographs of the specimens of the first set of experiments

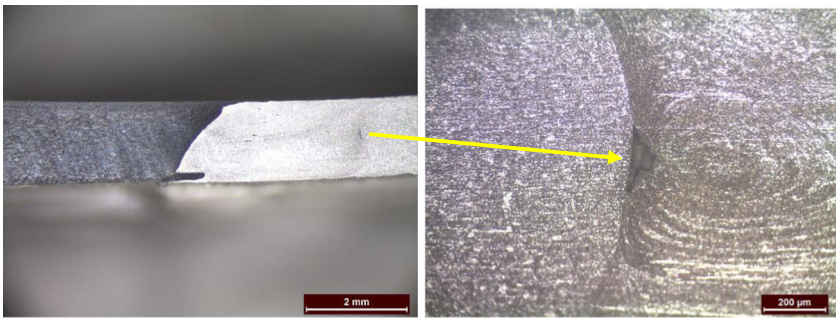

Fig. 3 Optical macrograph and micrograph of the weld nugget of the 600 RPM specimen

2.2 Welding procedure

A homemade-modified milling machine was used for the friction stir welding procedure. As it can be observed in Fig. 1a, a cemented carbide end mill was used as the basis of construction for the tool. After machining a 20-mm-wide shoulder with a geometry of a star-shaped polygon, a 4-mm-wide pin with a height of 1.8 mm was created (see Fig. 1b).

Regarding the choice of the welding parameters, only one suchlike study [14] exists in the literature

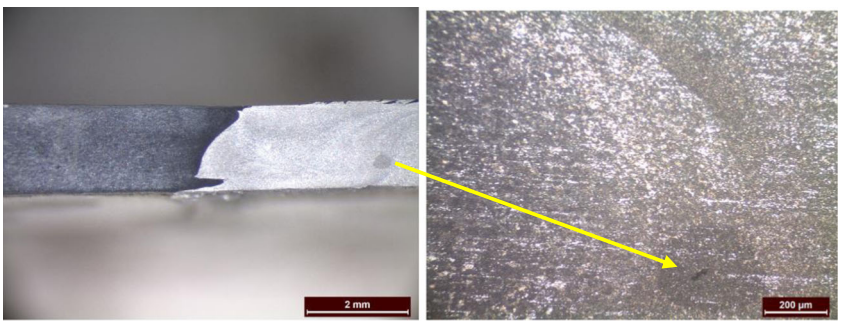

Fig. 4 Optical macrograph and micrograph of the weld nugget of the 950 RPM specimen

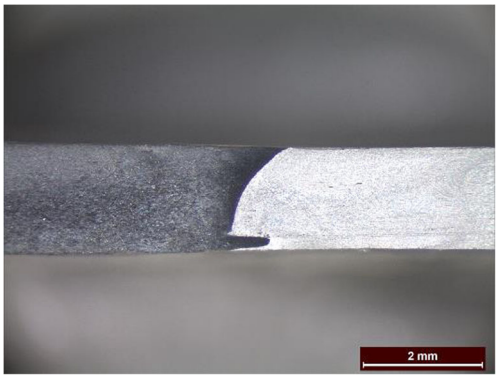

Fig. 5 Optical macrograph of the weld nugget of the 600 RPM specimen

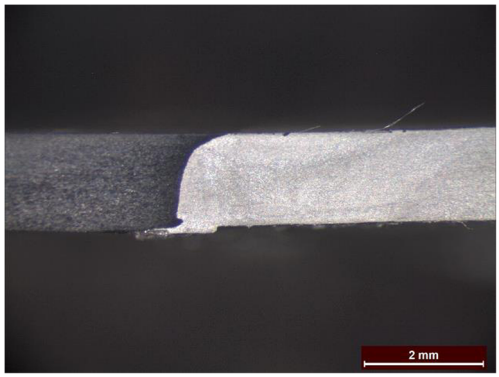

Fig. 7 Optical macrograph of the 750 RPM specimen

concerning the welding of 2-mm-thick plates of AA5083 to mild steel. In this study, it is concluded that a tool offset of only 0.2 mm into the steel provides the best results. In order to confirm that, the authors conducted a preliminary set of experiments placing the tool in three positions: (a) with an offset varying from 0.2 to 2 mm into the aluminum, (b) with an offset varying from 0.2 to 2 mm into the steel, and (c) in the middle of the weld line without any offset. Additionally, the authors tried a variety of different welding conditions. More specifically, the rotational speed was varied from 235 to 1500 RPM, while the traverse speed was varied from 19 to 75 mm/min. At this point, it should be mentioned that these parameters were selected based on the capabilities of the used FSW machine. Finally, the positioning of the aluminum alloy was also varied, i.e., it was placed on the advancing as well as the retreating side.

By studying all the aforementioned welds, the authors concluded that it is better for the AA5754 to be in the advancing side and the tool offset should be limited to 0.2 mm into the steel results that are in correlation with the literature [14]. Additionally, the rotational and the traverse speeds should be equal to or higher than 475 RPM and 30 mm/min respectively. Each set had a constant traverse speed but variable rotational speed. In all the experiments, the tool tilt angle was 2° and the aluminum was on the advancing side. At this point, the authors would like to point out that, as the traverse speed increased, the need for a higher thermal output, in order for the steel to be plasticized, rendered the conduction of low rotational speed experiments unnecessary. Based on the aforementioned results, four sets of experiments were proposed and conducted (see Table 2).

All the above welds were cut transversely to the welding direction and were prepared for metallographic observation. They were grinded and polished and then they were etched with the "modified Poulton's reagent." First, an optical stereoscope was used in order to determine the optimum specimens, and afterwards, an optical microscope was used in order to observe them thoroughly.

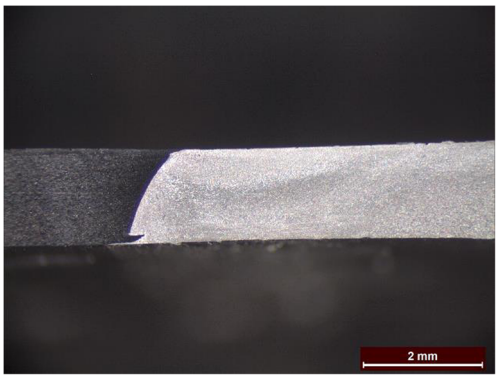

Fig. 6 Optical macrograph of the 750 RPM specimen

Table 3 Sound welds' parameters

No.	Traverse speed (v) (mm/min)	Rotational speed (ω) (RPM)	Weld pitch (v/ω) (mm/min / RPM)
1	30	600	0.05
2	30	750	0.04
3	30	950	0.03
4	47.5	750	0.06
5	60	750	0.08
6	75	750	0.10

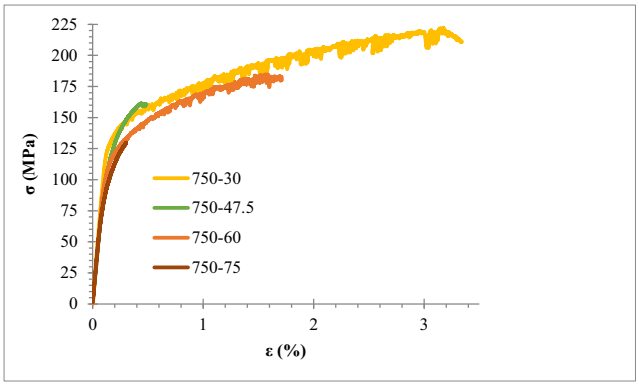

Fig. 8 Stress-strain curves of the optimum of the three tensile specimens of each case of all specimens

2.2.1 First set of experiments (30 mm/min traverse speed)

Regarding the first set of experiments, the 475 specimen presented groove-like defects and fractured during cutting. As a result, it was not further examined via optical microscopy. The rest of the specimens are presented in Fig. 2. All of them appear sound with a defect-free interface between the two materials.

2.2.2 Second set of experiments (47.5 mm/min traverse speed)

The optical macrographs and micrographs of the 600 RPM and the 950 RPM specimens are presented in Figs. 3 and 4 respectively. Although the two welds presented no obvious defects, both of them showed a small tunnel–like defect at the edge of the weld nugget at the advancing side, i.e., the aluminum side. The 750 RPM specimen is presented in Fig. 5 and it appears sound with a defect-free interface between the two materials.

2.2.3 Third set of experiments (60 mm/min)

Regarding the third set of experiments, the 950 RPM specimen presented a groove-like defect and fractured during cutting, and as a result, it was not further examined. The optical stereoscope image of the 750 RPM specimen is presented in Fig. 6. It appears sound with a defect-free interface between the two materials.

2.2.4 Fourth set of experiments (75 mm/min)

Regarding the fourth set of experiments, both welds appeared defect-free when observed with the naked eye. Still, during the cutting of the 950 RPM specimen, transversely to the welding direction, the plates were separated from one another, and as a result, it was not further examined. The optical stereoscope image of the 750 RPM specimen, which was sound and did not fracture during cutting, is presented in Fig. 7. It appears sound with a defect-free interface between the two materials.

Summarizing, all the sound welds are presented in Table 3.

As it can be observed, the no. 1, no. 2, and no. 3 sets of parameters present very little weld pitch variation. As a result, the authors decided to further test only specimen no. 2 which provides an average weld pitch value. Additionally, the specimens no. 4, no. 5, and no. 6 are also going to be examined, i.e., the ones with a 750 RPM rotational speed. Each one also provides a 0.2 mm/min / RPM weld pitch step.

3 Results and discussion

3.1 Tensile testing

Thereinafter, in order to determine the set of welding parameters that results in a strong and durable weld, tensile testing was firstly conducted. The tensile specimens were machined

Table 4 Mechanical properties of the specimens

Specimen no.	Parameters	UTS (MPa)	YS (MPa)	Elongation (%)	Toughness (J/m3)	Area of fracture
2	750 30	222.30 ± 11.7	150.5 ± 7.4	3.12 ± 0.6	621.86 ± 11.2	HAZ
4	750 47,5	161.55 ± 7.6	140 ± 5.2	0.31 ± 0.1	58.39 ± 4.4	WN
5	750 60	184.80 ± 4.2	128.4 ± 2.2	1.56 ± 0.3	262.89 ± 7.8	WN
6	750 75	129.90 ± 7.4	92 ± 5.1	0.17 ± 0.2	27.21 ± 3.1	WN
AA5754 BM	–	240.93 ± 3.7	137 ± 2.8	16.00 ± 0.8	–	–
Mild steel BM	–	440	370	15.00	–	–

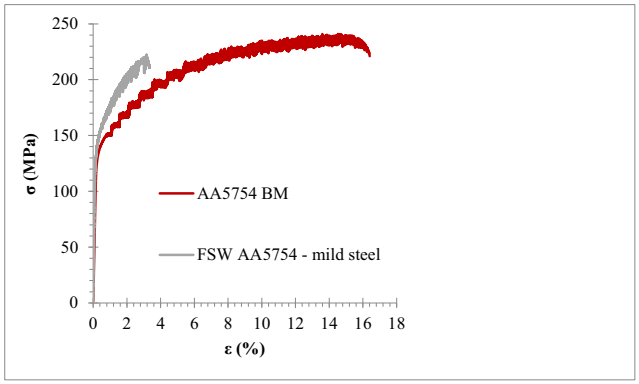

Fig. 9 Stress-strain curve comparison

from the aforementioned plates according to the ASTM E 8M-04 standard perpendicular to the welding direction. A hydraulic mechanical testing machine was used to perform the tensile tests. The maximum load of the machine was 100 kN. In order to assure the repeatability of the measurements, the authors machined three specimens from each weld. The deformation speed was 0.5 mm/min and an Epsilon ± 25 mm extensometer was used in order to measure the elongation.

A comparison of the stress-strain curves of the optimum of the three tensile specimens of each case of all the aforementioned specimens is presented in Fig. 8. The values for the yield stress (YS), ultimate tensile strength (UTS), and percentage of elongation are presented in Table 4. The mechanical properties of the AA5754 base metal are also presented in Table 4, along with the equivalent of the mild steel base metal (for comparison purposes). The only set of specimens that fractured in the heat-affected zone (HAZ) and not in the weld nugget is the one of the 750-30 specimen. Fracturing in the HAZ proves that the material bonding is good and that the weakest point of the weld is outside the weld nugget.

The toughness (i.e., the area underneath the stress-strain curve [19–23], which represents the energy per volume unit required to cause rupture to the material) of the welded specimens is also presented in Table 4. As expected, the 750-30 specimen that presents the best tensile behavior presents also the highest modulus of toughness.

By observing Table 4, it is clear that the specimen no. 2 provides the best overall tensile behavior. As it was expected, the weld's tensile behavior is not comparable to the equivalent of the mild steel base metal. On the other hand, in Fig. 11, a comparison between the stress-strain curves of the optimum weld and the AA5754 base metal is presented. The percentage of elongation is far greater in the base metal. FSW appears to have made the material much more brittle compared to the base metal. This degradation of the mechanical properties is characteristic of the aluminum-steel dissimilar friction stir welds as it has also been observed by Jiang et al. [13] and Watanabe et al. [14]. This decrease in the maximum elongation of the specimen occurs even in the case of similar AA5754 FSW as it is demonstrated by Cabibbo et al. [24] and Gabrielli et al. [25]. Lastly, both the aluminum alloy base metal and the dissimilar weld specimens present Portevin–Le Chatelier effect and shear banding as indicated by the serrated stress-strain curves (see Fig. 9), something that was expected by studying the literature [26].

In Fig. 10, the fracture surface of the optimum specimen no. 2 is presented. As it fractured in the HAZ and not in the WN, it presents the typical for aluminum alloys ductile fracture surface with small dimples.

3.2 Scanning electron microscopy and energy dispersive spectroscopy study

A comparison study was conducted between the optimum welded specimen no. 2 and the specimen no. 5

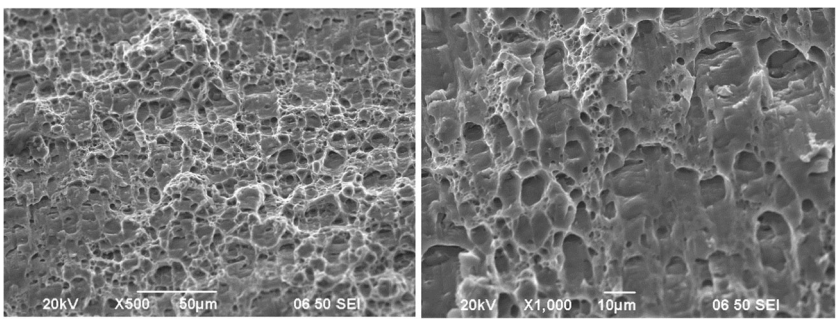

Fig. 10 Scanning electron micrographs of the fracture surface at the HAZ of the 750–30 specimen. **a** × 500. **b** × 1000

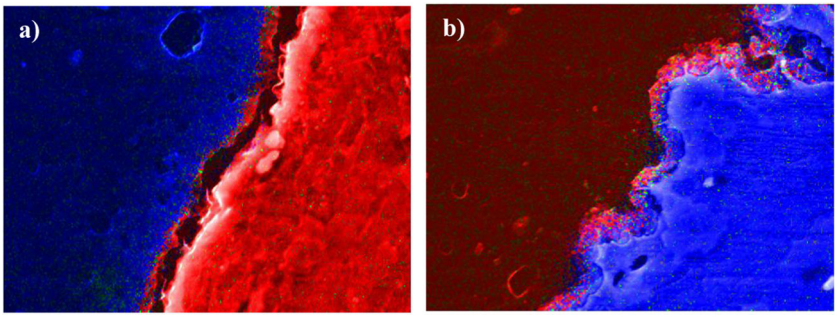

Fig. 11 EDS area mapping at the weld nugget of the **a** specimen no. 2 and **b** specimen no. 5

which presented the second higher UTS and elongation (see Table 3) but fractured in the WN in an attempt to find out the cause of the better bonding in the case of specimen no. 2. It was conducted separately for three distinct regions of the weld nugget, i.e., the upper, the middle, and the lower, using a scanning electron microscope equipped with an energy dispersive spectroscopy system. Although several EDS mapping lines were conducted, only a representative one for each region is going to be presented with a view to avoid unnecessary repetition.

Firstly, one representative EDS area mapping was conducted for each specimen (see Fig. 11). As it can be observed by the color mixing (in both cases, the material on the left side is the aluminum), the existence of an interdiffusion layer at the interface of the two alloys is apparent. The authors speculate that, in this interdiffusion layer, the two materials are just mechanically mixed and have not reacted with each other (generating Fe-Al bimetallic phases). This is due to the fact that the peak temperature during FSW does not exceed 550 °C [27] and, as it can be observed by the iron-aluminum phase diagram (see Fig. 12), it is not enough in order to result in the phase transformation of the materials.

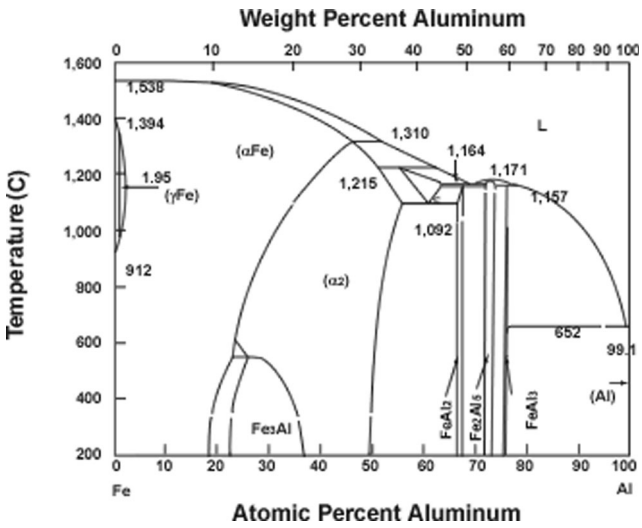

Fig. 12 The iron-aluminum phase diagram from [www.researchgate.net]

Afterwards, the EDS line mapping study followed in order to determine and compare the width of the aforementioned interdiffusion layers in both specimens. In order to be able to draw robust results, independent line measurements were conducted for the upper (0.5 mm from the tool shoulder surface), middle (1 mm from the tool shoulder surface), and lower (1.5 mm from the tool shoulder surface) region of the specimens' interface (see Fig. 13).

Regarding the upper region of the weld nugget, as it can be observed in Fig. 13a and b, an interdiffusion layer was created that presents a combination of aluminum, magnesium, and iron which are the major alloying elements of the AA5754 and the mild steel respectively. The width of this layer, indicated by the dotted lines on the diagrams, is 5.5 μm for the case of the specimen no. 2 and 3 μm for specimen no. 5. The optimum specimen no. 2 presents a wider interdiffusion layer. The authors speculate that this may be due to the fact that specimen no. 2 presents a lower weld pitch compared to specimen no. 5 (see Table 3), and as a result, the materials were further heated and plasticized which in turn led to the further mechanical mixture of the two materials. Regarding the middle region of the weld nugget of specimen no. 2 and specimen no. 5, as it can be observed in Fig. 13c and d, the interdiffusion layer width is 5 μm for the case of the specimen no. 2 and 3 μm for specimen no. 5. As in the case of the upper region examination, the optimum specimen no. 2 again presents a wider interdiffusion layer. Finally, concerning

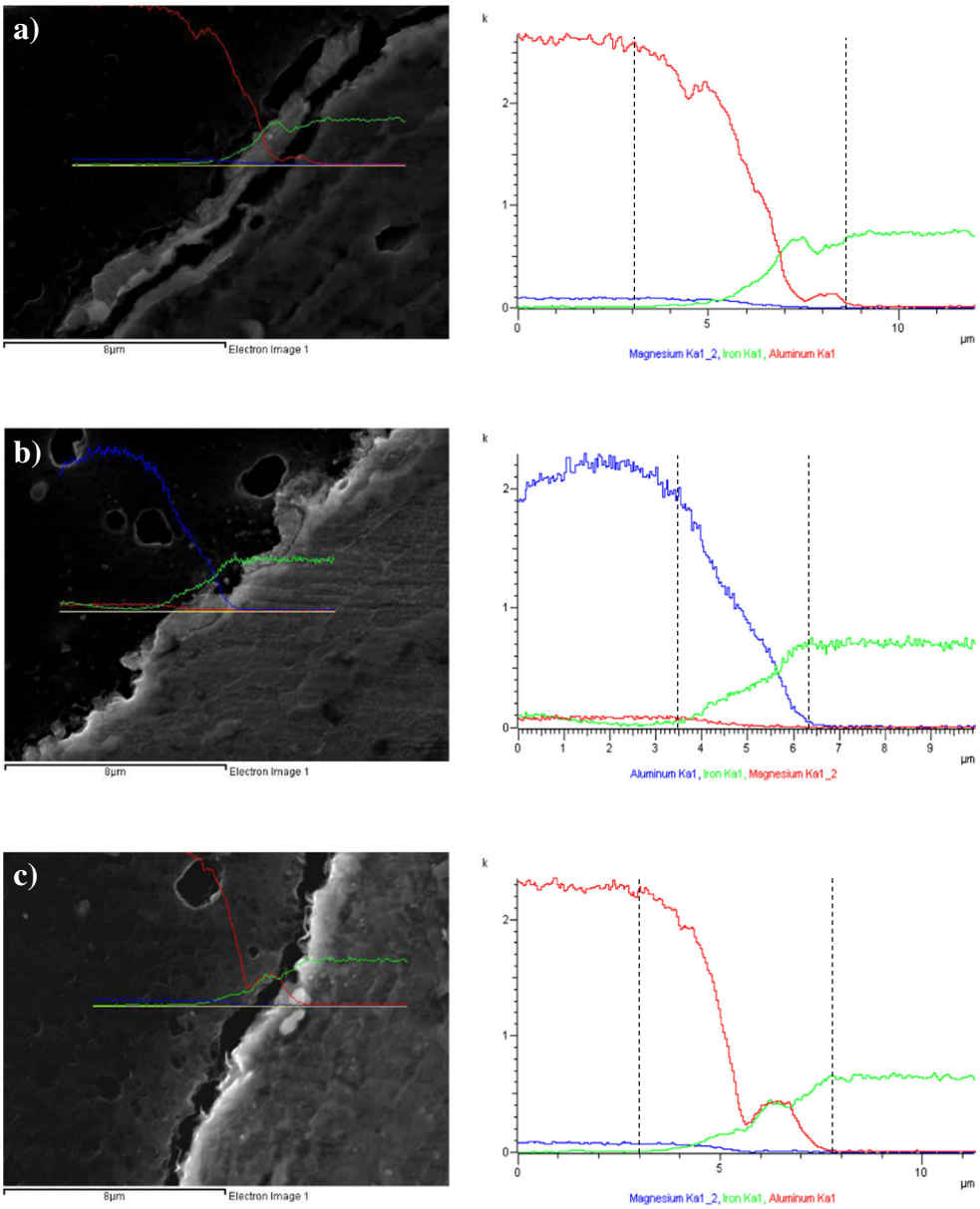

Fig. 13 Scanning electron micrograph and EDS line mapping of **a** the upper region of the optimum specimen no. 2 (red-aluminum, green-steel, blue-magnesium), **b** the upper region of specimen no. 5 (blue-aluminum, green-steel, red-magnesium), **c** the middle region of the optimum specimen no. 2 (red-aluminum, green-steel, blue-magnesium), **d** the middle region of specimen no. 5 (green-aluminum, blue-steel, red-magnesium), **e** the lower region of the optimum specimen no. 2 (red-aluminum, blue-steel, green-magnesium), and **f** the lower region of specimen no. 5 (blue-aluminum, green-steel, red-magnesium)

the lower region, as it can be observed in Fig. 13e and f, the interdiffusion layer width is 4 μm for the case of the specimen no. 2 and 3 μm for specimen no. 5. As in the case of both the upper and middle region examination, the optimum specimen no. 2 again presents a wider interdiffusion layer.

The overall results are presented in Table 5. At this point, it should be mentioned that these results are in the average of the measurements conducted to the plethora of the EDS mapping lines that were scanned at every region of the weld nugget.

As it can be clearly observed, the interdiffusion layer is significantly wider in the case of the optimum specimen no. 2. That led the authors to conclude that this is the reason for the better bonding which provides the better mechanical properties of the weld as explained in previous paragraphs.

Additionally, several point ID EDS studies were conducted in order to determine the composition of the interdiffusion layer with a characteristic one being presented in Fig. 14. Unfortunately, no robust conclusion can be drawn as the only elements that are detected are iron,

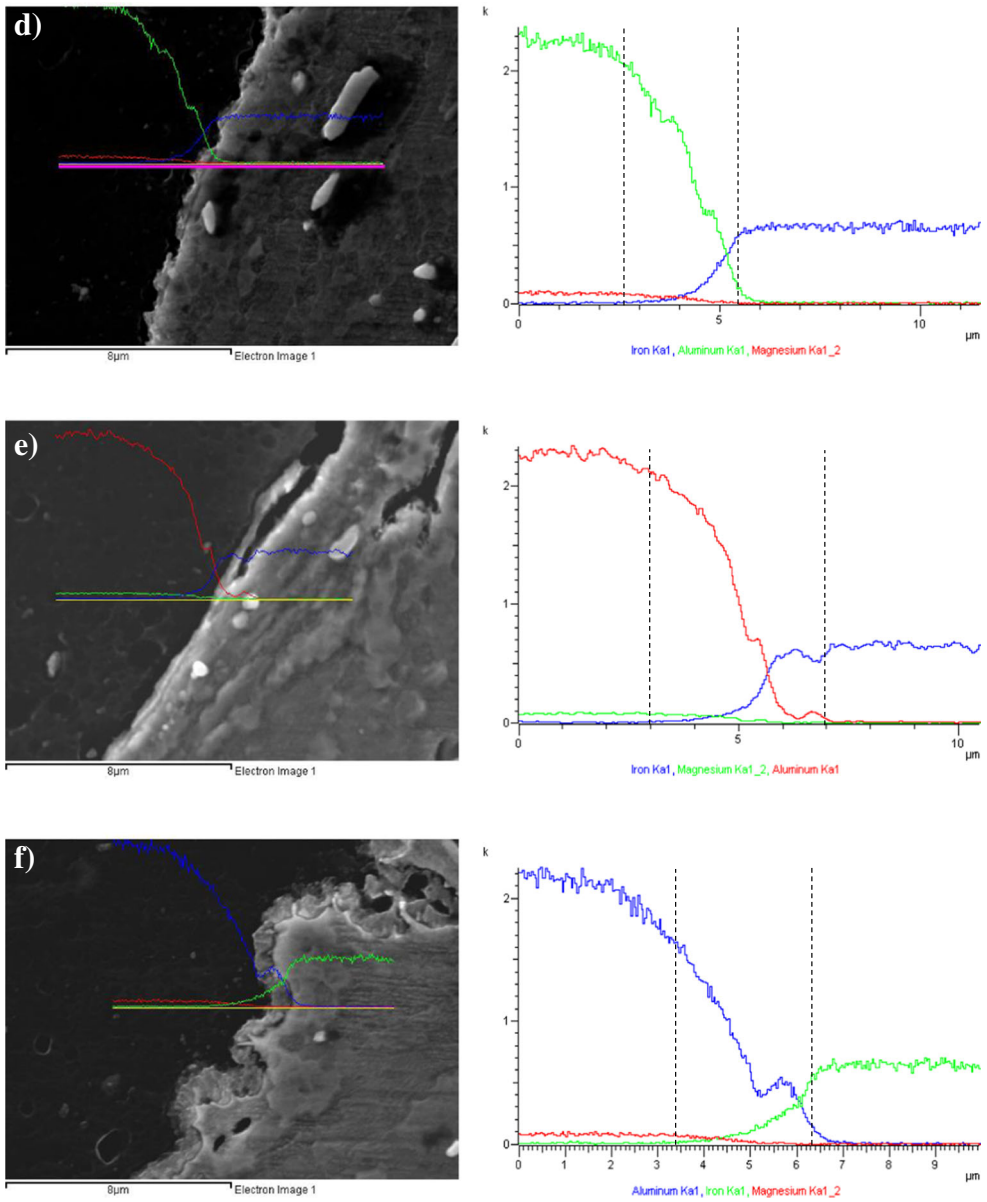

Fig. 13 (continued)

aluminum, and magnesium (as the AA5754 is a solid solution).

Table 5 Interdiffusion layer width (in µm)

Specimen	Upper region	Middle region	Lower region
No. 2 (optimum)	5.5	5	4
No. 5	3	3	3

3.3 Microhardness distribution

In addition, microhardness measurements of the optimum weld no. 2 were conducted and presented in Fig. 15. For this reason, a Vickers microhardness tester was used. The longitudinal microhardness distribution was defined at 0.75 mm below the surface of the plates that is in contact with the tool shoulder, i.e., the mid-thickness plane. A 300-g load was used.

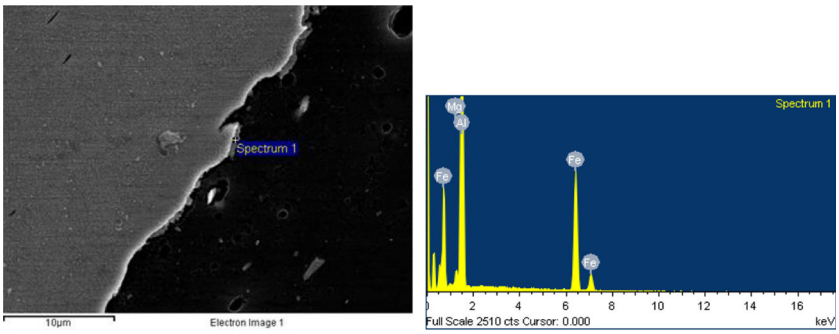

Element	Weight%	Atomic%
Mg K	1.27	1.77
Al K	60.01	74.89
Fe K	38.71	23.34
Totals	*100.00*	

Fig. 14 EDS point ID chemical analysis of the interdiffusion layer

The microhardness values of the base metal AA5754 and mild steel are 60 HV and 130 HV respectively. Regarding the mild steel side, i.e., the retreating side (RS), the hardness values in the weld nugget are about 40% higher compared to the mild steel base metal. In this region, dynamic recrystallization (DRX) has occurred [28, 29] which led to the refinement and the decrease of the dislocation density of the grains. Had this mechanism been acting alone, there should have been a decrease in this region's hardness. Nevertheless, the grain refinement can be beneficial to the mechanical properties and the microhardness of a material as the Hall-Petch strengthening suggests [30]. As a result, the authors concluded that the two aforementioned mechanisms act simultaneously but the Hall-Petch mechanism takes precedence.

The microhardness drops as we move towards the HAZ, where the material presents slightly lower hardness compared to the base metal. Although this difference is within the measurement error margins, it might be caused by the annealing due to the heat imparted by the tool. Concerning the AA5754 side, i.e., the advancing side (AS), the microhardness is a little higher than the equivalent of the base metal in all zones. That might be due to the formation of harder second phase particles caused by the thermal cycle of friction stir welding (temperature rise and subsequent cooling). Nevertheless, it is within the measurement error margins. The overall variation range of the microhardness values due to the different trials that were conducted was around 8%, demonstrating the very good repeatability of the experiments.

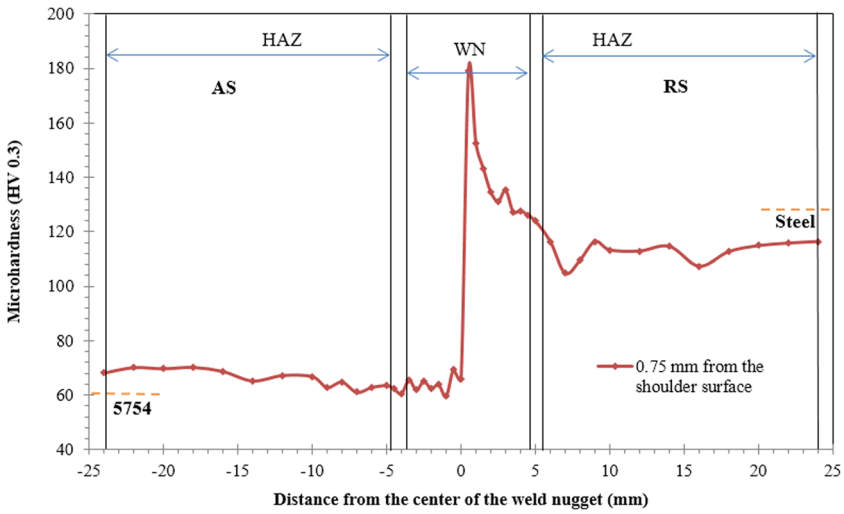

Fig. 15 Microhardness distribution of the specimen No 2

4 Conclusions

This study focused on the feasibility of using the friction stir method in order to achieve dissimilar butt welding between 2-mm-thick plates made of the automotive grade AA5754-H114 and mild steel. The specimens were studied via optical and electron microscopy as well as tensile and microhardness testing. The following conclusions were drawn:

- The optimum parameters for achieving the aforementioned welding are 750 RPM rotational speed, 30 mm/min traverse speed, 0.2 mm tool offset into steel, and the AA5754 on the advancing side. It should be noted that this welding parameter set is only optimum for the corresponding joint thickness of 2 mm.
- The optimum weld presented a UTS and YS very close to the equivalent of the aluminum base metal but lower elongation. Nevertheless, these results correlate with the ones of similar studies in the literature.
- The optimum weld, which fractured in the heat-affected zone, presented a wider interdiffusion layer compared to the welds that fractured in the weld nugget. This wide layer is probably the cause of the better bonding between the two materials.
- The microhardness rise in the weld nugget is in correlation with the grain refinement (Hall-Petch strengthening) caused by the dynamic recrystallization that took place in this region.

Acknowledgments The authors thank the European Commission for their support on the H2020 project "Low Cost Materials Processing Technologies for Mass Production of Lightweight Vehicles (LoCoMaTech)," Grant No: H2020-NMBP- GV-2016 (723517).

References

1. Dawes CJ, Thomas WM (1996) Friction stir process welds aluminum alloys. Weld J 75(3):41–45
2. Golezani AS, Barenji RV, Heidarzadeh A, Pouraliakbar H (2015) Elucidating of tool rotational speed in friction stir welding of 7020-T6 aluminum alloy. Int J Adv Manuf Technol 81(5–8):1155–1164
3. Charitidis CA, Dragatogiannis DA, Koumoulos EP, Kartsonakis IA (2012) Residual stress and deformation mechanism of friction stir welded aluminum alloys by nanoindentation. Mater Sci Eng A 540: 226–234
4. Koumoulos EP, Charitidis CA, Daniolos NM, Pantelis DI (2011) Nanomechanical properties of friction stir welded AA6082-T6 aluminum alloy. Mater Sci Eng B 176(19):1585–1589
5. Daniolos NM, Pantelis DI (2017) Microstructural and mechanical properties of dissimilar friction stir welds between AA6082-T6 and AA7075-T651. Int J Adv Manuf Technol 88(9–12):2497–2505
6. Leitão C, Louro R, Rodrigues DM (2012) Analysis of high temperature plastic behaviour and its relation with weldability in friction stir welding for aluminium alloys AA5083-H111 and AA6082-T6. Mater Des 37:402–409
7. Heidarzadeh A, Pouraliakbar H, Mahdavi S, Jandaghi MR (2018) Ceramic nanoparticles addition in pure copper plate: FSP approach, microstructure evolution and texture study using EBSD. Ceram Int 44(3):3128–3133
8. Dragatogiannis DA, Koumoulos EP, Kartsonakis I, Pantelis DI, Karakizis PN, Charitidis CA (2016) Dissimilar friction stir welding between 5083 and 6082 Al alloys reinforced with TiC nanoparticles. Mater Manuf Process 31(16):2101–2114
9. Pantelis DI, Karakizis PN, Daniolos NM, Charitidis CA, Koumoulos EP, Dragatogiannis DA (2016) Microstructural study and mechanical properties of dissimilar friction stir welded AA5083-H111 and AA6082-T6 reinforced with SiC nanoparticles. Mater Manuf Process 31(3):264–274
10. Pantelis DI, Karakizis PN, Dragatogiannis DA, Charitidis CA (2015) Dissimilar friction stir welding of aluminum alloys reinforced with carbon nanotubes. In: Charitidis CA (ed) Nanomaterials in joining, 1st edn. de Gruyter, Berlin, pp 23–52
11. Amirafshar A, Pouraliakbar H (2015) Effect of tool pin design on the microstructural evolutions and tribological characteristics of friction stir processed structural steel. Measurement 68:1–336
12. Uzun H, Donne CD, Argagnotto A, Ghidini T, Gambaro C (2005) Friction stir welding of dissimilar Al 6013- T4 to X5CrNi18-10 stainless steel. Mater Des 26:41–46
13. Jiang WH, Kovacevic R (2004) Feasibility study of friction stir welding of 6061-T6 aluminium alloy with AISI 1018 steel. Proc Inst Mech Eng B J Eng Manuf 218(10):1323–1331. https://doi.org/10.1243/0954405042323612
14. Watanabe T, Takayama H, Yanagisawa A (2006) Joining of aluminum alloy to steel by friction stir welding. J Mater Process Technol 178:342–349
15. Tanaka T, Morishige T, Hirata T (2009) Comprehensive analysis of joint strength for dissimilar friction stir welds of mild steel to aluminum alloys. Scr Mater 61:756–759
16. Sajin GS, Manish M, Pankaj, Srinivas P, Dey SR (2013) Friction stir welding of aluminum 6082 with mild steel and its joint analyses. Conference Paper Advanced Materials International Journal Of Advanced Materials Manufacturing and Characterization (3)1, 3: 189–193
17. Thomä M, Wagner G, Straß B, Wolter B, Benfer S, Fürbeth W (2018) Ultrasound enhanced friction stir welding of aluminum and steel: process and properties of EN AW 6061/DC04-Joints. Mater Sci Technol 34(1):163–172. https://doi.org/10.1016/j.jmst.2017.10.022
18. Tang J, Shen Y (2017) Effects of preheating treatment on temperature distribution and material flow of aluminum alloy and steel friction stir welds. J Manuf Process 29:29–40
19. Jandaghi MR, Pouraliakbar H, Khalaj G, Khalaj M-J, Heidarzadeh A (2016) Study on the post-rolling direction of severely plastic deformed aluminum-manganese-silicon alloy. Arch Civil Mech Eng 16:876–887
20. Jandaghi MR, Pouraliakbar H (2017) Study on the effect of post-annealing on the microstructural evolutions and mechanical properties of rolled CGPed aluminum-manganese-silicon alloy. Mater Sci and Eng: A 679:493–503

21. Pouraliakbar H, Jandaghi MR, Khalaj G (2017) Constrained groove pressing and subsequent annealing of Al-Mn-Si alloy: microstructure evolutions, crystallographic transformations, mechanical properties, electrical conductivity and corrosion resistance. Mater and Des 124:34–46
22. Pouraliakbar H, Jandaghi MR, Heidarzadeh A, Jandaghi MM (2018) Constrained groove pressing, cold-rolling, and post-deformation isothermal annealing: consequences of their synergy on material behavior. Mater Chem Phys 206:85–93
23. Khorrami MS, Mostafaei MA, Pouraliakbar H, Kokabi AH (2014) Study on microstructure and mechanical characteristics of low-carbon steel and ferritic stainless steel joints. Mater Sci and Eng: A 608:35–45
24. Cabibbo M, Forcellese A, Simoncini M, Pieralisi M, Ciccarelli D (2016) Effect of welding motion and pre-/post-annealing of friction stir welded AA5754 joints. Mater Des 93:146–159
25. Gabrielli F, Forcellese A, El Mehtedi M, Simoncini M (2017) Mechanical properties and formability of cold rolled friction stir welded sheets in AA5754 for automotive applications. Procedia Eng 183:245–250
26. Halim H, Wilkinson DS, Niewczas M (2007) The Portevin–Le Chatelier (PLC) effect and shear band formation in an AA5754 alloy. Acta Mater 55:4151–4160
27. Silva ACF, De Backer J, Bolmsjö G (2017) Temperature measurements during friction stir welding. Int J Adv Manuf Technol 88(9–12):2899–2908
28. McNelley TR, Swaminathan S, Su JQ (2008) Recrystallization mechanisms during friction stir welding=processing of aluminum alloys. Scr Mater 58(5):349–354
29. Humphreys FJ, Hatherly M (2004) Recrystallization and related annealing phenomena. Elsevier, Oxford
30. Bahrami M, Dehghani K, Kazem Besharati Givi M (2014) A novel approach to develop aluminum matrix nano-composite employing friction stir welding technique. Mater Des 53:217–225